Tatikonda, Rajendhraprasad; Bulatov, Evgeny; Özdemir, Zulal; Nonappa, Nonappa; Haukka, Matti

Infinite coordination polymer networks

Published in:
Soft Matter

DOI:
10.1039/c8sm02006j

Published: 01/01/2019

Document Version
Peer-reviewed accepted author manuscript, also known as Final accepted manuscript or Post-print

Please cite the original version:
Tatikonda, R., Bulatov, E., Özdemir, Z., Nonappa, N., & Haukka, M. (2019). Infinite coordination polymer networks: metallogelation of aminopyridine conjugates and in situ silver nanoparticle formation. *Soft Matter*, *15*(3), 442-451. https://doi.org/10.1039/c8sm02006j

Journal Name

ARTICLE

Infinite coordination polymer networks: Metallogelation of aminopyridine conjugates and *in situ* silver nanoparticle formation†

Received 00th January 20xx,
Accepted 00th January 20xx

DOI: 10.1039/x0xx00000x

www.rsc.org/

Rajendhraprasad Tatikonda,[a] Evgeny Bulatov,[a] Zülal Özdemir,[d] Nonappa,*[b,c] and Matti Haukka*[a]

Herein we report silver(I) directed infinite coordination polymer network (ICPN) induced self-assembly of low molecular weight organic ligands leading to metallogelation. Structurally simple ligands are derived from 3-aminopyridine and 4-aminopyridine conjugates which are composed of either pyridine or 2,2´-bipyridine cores. The cation specific gelation was found to be independent of the counter anion, leading to highly entangled fibrillar networks facilitating the immobilization of solvent molecules. Rheological studies revealed that the elastic storage modulus (*G´*) of a given gelator molecule is counter anion dependent. The metallogels derived from ligands containing bipyridine core displayed higher *G´* values than those with pyridine core. Further, using single crystal X-ray diffraction studies and ^{1}H-^{15}N two-dimensional (2D) correlation NMR spectroscopy, we show that the tetracoordination of silver ions enable simultaneous coordination polymerization and metallosupramolecular cross-linking. The resulting metallogels show spontaneous, *in-situ* nanoparticle (d <2-3 nm) formation without any additional reducing agents. The silver nanoparticle formation was followed using spectroscopic studies and the self-assembled fibrillar networks were imaged using transmission electron microscopy (TEM) imaging.

Introduction

Metal-ligand (M-L) interaction induced assembly of small organic molecules (i.e. metallosupramolecular chemistry) evolved as one of the versatile ways to build topologically diverse metallosupramolecular structures.[1] The ability to tune the interaction strength, number of metal binding sites with synthetically simple organic ligands offer rapid access to one, two, or three-dimensional metallosupramolecular polymeric structures.[2] In certain cases, the resulting superstructures undergo hierarchical assembly to highly entangled fibrillar networks and immobilize the solvents leading to gelation. The resulting gels are known as metallosupramolecular gels or simply metallogels.[3] Metallogels are either produced from discrete coordination compounds,[4] infinite coordination polymers (ICPs),[5] or cross-linked CPs[6]. In discrete metal complexes, the supramolecular interactions between the gelator molecules promote the self-assembly, whereas the metal-ligand coordination often acts as a secondary force in gelation. Gels derived from discrete complexes display reversible gel-sol transition upon subjecting them to external stimuli (e.g., temperature, light, pH etc). On the other hand, in coordination polymers (CPs), the major driving force is metal-ligand coordination, leading to infinite coordination polymeric networks (ICPNs) and the coordination polymers act as gelators. The gels derived from ICPs often show resistance to reversible gel-sol transition.[7] The presence of metal ions provides some of the unique responsiveness to temperature,[8] mechanical perturbance,[9] light,[10] oxidation-reduction,[11] electric- and magnetic fields[12]. The structure and coordination ability of organic ligand has an impact on topologies and functional properties of metal complexes. Therefore, selection of organic ligand is vital in preparing functional metallogels, where crystal engineering approach has played an important role. Ligands containing different metal binding sites have been studied in metallogelation, for example, polypyridyl compounds, porphyrin derivatives, amines, thiols, azoles, dendrimers, and carboxylates.[13-17] In order to obtain a metallogel, ligand should able to participate in one or more than one noncovalent intermolecular interactions (such as H-bonding, π-stacking, van der Waals interaction, electrostatic interactions) in addition to metal coordination.[18] Various approaches have been reported in the literature on the preparation of metallogels, including subcomponent self-assembly.[19] Potential applications of metallogels in cosmetics, lubrication, magnetic materials and sensors for dye molecules have been demonstrated in the literature.[20-22] Further, properties such as the self-assembly induced luminescence provides promising applications in

[a] *Department of Chemistry, University of Jyväskylä, P. O. Box 35, FI-40014 Jyväskylä, Finland. E-mail: matti.o.haukka@jyu.fi.*
[b] *Department of Applied Physics, Aalto University School of Science, Puumiehenkuja 2, FI-02150 Espoo, Finland. E-mail:nonappa@aalto.fi*
[c] *Department of Bioproducts and Biosystems, Aalto University School of Chemical Engineering, Kemistintie 1, FI-02150 Espoo, Finland.*
[d] *University of Chemistry and Technology in Prague, Faculty of Food and Biochemical Technology Department of Chemistry of Natural Compounds Technicka 5, 16628 Prague 6, Czech Republic*

†Electronic Supplementary Information (ESI) available: [Synthesis of ligands, 1D and 2D NMR spectra of ligands and their silver complexes, single crystal X-ray data, additional TEM micrographs and rheological and photoluminescence studies]. See DOI: 10.1039/x0xx00000x

optoelectronics[23] and in developing vapochromic sensors[24]. Recently, terpyridine ligands containing perfluoroalkyl chains have been reported to exhibit anion selective gelation and rapid self-healing properties.[25] The transition metal containing gels such as palladium have also been shown to improve the catalytic activities.[26]

Metallogels containing Ag(I) as metal ions and pyridine derivatives as ligands, represent one of the extensively studied systems. This is attributed to their antimicrobial and photophysical properties.[27] In addition to its role as coordinating agent, Ag(I) also serves as a precursor for *in-situ* silver nanoparticle (AgNP) formation without any additional stabilizing agents.[28] *In-situ* silver nanoparticle (AgNP) formation in metallogels involving pyridine and bipyridyl molecules have been reported either under ambient conditions, UV irradiation or sodium borohydride reduction.[29,30] However, in a majority of the reports, the resulted AgNPs were relatively large (>5 nm). We have recently reported synthetically simple bipyridyl based gelators displaying a remarkable difference in their ability to size and shape selective AgNP formation depending on the source of reducing agent and gelator chemical structure.[31] Further, the binding of Ag(I) to form polymeric structures *via* tetracoordination of Ag(I) has been proposed based on 2D NMR spectroscopic studies. Understanding the exact metal-ligand interaction in hierarchical structure formation is important not only to gain insights on the gelation mechanism but also in the rational design of materials with desired morphology and mechanical properties.

ICPs have been studied mostly in the context of crystal engineering. Further, it has been shown that structurally complex ligands prepared using sophisticated ligand design allow tailorable colloidal microparticle formation with spherical morphologies.[32] Beyond crystal engineering and structure formation, there is a need to design strategically simple ligands for ICPN formation to provide access to novel multifunctional hybrid materials.

In this work, we report the synthesis, infinite coordination polymerization directed gelation, self-assembly induced luminescence and *in-situ* silver nanoparticle ($d \leq 3$ nm) formation of pyridyl and bipyridyl amides (**1–4**) in aqueous dimethyl sulfoxide (Fig. 1). Using single crystal X-ray diffraction studies we show that, tetracoordinated silver is responsible for metallosupramolecular polymerization in the solid state. Further, the metal complexes in solution were studied using ^{1}H-^{15}N 2D NMR spectroscopy. Importantly, silver(I) directs, coordination polymerization (CP), supramolecular cross-linking between the polymeric chains thereby leading to highly entangled fibrillar network formation and also acts as a source for ultrasmall AgNPs. The gelation is cation specific and their stability depends on the counter anion.

Results and discussion

The pyridyl amide ligands (**1** and **2**) were synthesized according to the reported literature procedure.[33] The synthesis of bipyridyl amide ligands (**3** and **4**) was achieved by the reaction of 4,4′-dicarboxy-2,2′-bipyridine with 3-, or 4-aminopyridines in the presence of *N*-ethyl-*N*'-(3-dimethylaminopropyl carbodiimide (EDC) in *N*, *N*-dimethyl formamide (DMF) solvent (see ESI, Scheme S1 and Figs. S1-S10 for NMR spectral data).

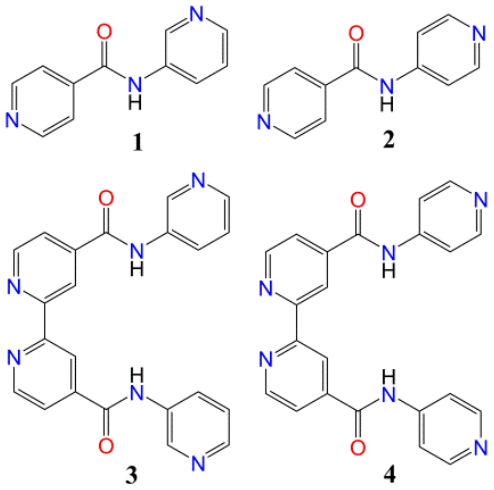

Figure 1. Chemical structure of ligands used in this study.

First, we discuss the structural properties of ligands **1–4** (Fig. 1). The solid-state structural details of ligands **1–2** have already been documented in the literature.[34] Therefore, no attempts were made to obtain their single crystals. Instead, efforts were made to grow single crystals and determine X-ray structures of ligands **3** and **4**. However, only ligand **4** was resulted in quality single crystal either from acetonitrile, dimethyl sulfoxide (DMSO) or *N, N*- dimethylformamide (DMF) (Fig. 2).[35]

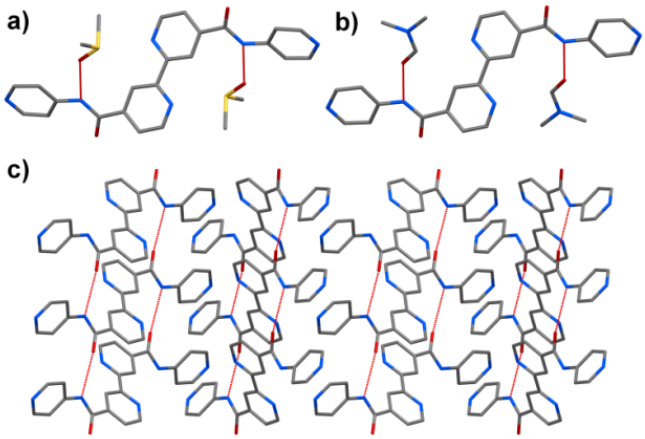

Figure 2. X-ray single crystal structure: A molecular unit of **4** recrystallized from DMSO (a), DMF (b) and crystal packing of well-organized H-bonding in **4** recrystallized from acetonitrile (c). Hydrogen atoms are omitted for clarity.

Ligand **3** either remained in solution or resulted in a precipitate. The solid-state structure of **4** obtained from acetonitrile (Fig. 2c) shows well organized intermolecular H-bonding (N–H···O = 2.18 Å) between the adjacent molecules through amide groups. The crystal packing also reveals that the presence of weak intermolecular aromatic C=C–H···N and C=C–H···O H-bonding interactions. In addition to these weak H-bonds, the packing commences through off-set π···π interactions (3.3 Å). When ligand **4** was crystallized from DMSO (Fig. 2a) or DMF (Fig. 2b),

solvates were obtained, and the ligand molecule participated in H-bonding with the oxygen atom of solvent molecules.

Ligands **1** and **2** have been previously studied for their hydrogelation ability without the addition of metal ions by Das *et al*., and their experimental results have shown that only **2** was able to form a hydrogel.[34] Importantly, the previous study was carried out only in water and not using any solvent mixtures. In this study, ligands **1**-**4** are screened for gelation and metallogelation. First ligand **1** was tested in ethanol, acetonitrile, tetrahydrofuran, N, N´-dimethyl formamide (DMF), dimethyl sulfoxide (DMSO) and their mixture with water. In all the tested solvents, ligand **1** remained soluble. However, when a mixture of DMSO:H_2O or DMF:H_2O (2:8 or 3:7 v/v) the pure ligand resulted in crystals and similar results were observed from ligand **2** (Fig. S11). Ligand **3** and **4** on the other hand were insoluble in tested solvents except in DMSO and DMF. Further, when a mixture of DMSO:H_2O or DMF:H_2O was used, ligand **3** and **4** resulted in precipitates. The presence of tertiary nitrogen offers metal binding sites in all the four ligands, therefore, it is interesting see how the metal complexation affects the assembly of the ligands. In order to test this hypothesis various water soluble metal salts were tested. Among all the tested metal ions, complexation with silver (I) ions furnished metallogels in aqueous DMSO or aqueous DMF indicating the cation specific metallogelation properties of the ligands. Therefore, systematic studies using six different silver salts *viz*. nitrate (NO_3^-), trifluoromethane sulfonate aka triflate (OTf^-), perchlorate (ClO_4^-), acetate (OAc^-), tetrafluoroborate (BF_4^-) and hexafluorophosphate (PF_6^-) were performed. Table 1 and Figure 3 show the details of gelation studies of ligands **1**-**4** when mixed with different silver salts and corresponding photographs in a given ratio of DMSO:H_2O system, respectively.

The metallogelation was studied for bidentate ligand **1** in 2:8, 3:7 and 4:6 DMSO:H_2O (v/v) ratio. However, stable metallogels were obtained in 3:7 DMSO:H_2O. It should be stated that the solvent mixture has an impact on metallogelation and no gelation was observed in pure DMSO or when the volume of DMSO was higher than the water in a mixture. Similar results were obtained for ligand **2**. In order to find out the optimum ligand to metal mole ratio, gelation studies were carried out using silver nitrate at 4:1, 2:1 and 1:1 ligand to metal (L:M) ratio.

Table 1. Gelation studies of ligands **1−4** with various silver salts in a mixture of water and DMSO. (Note: **G**= gel, **G***= gels are unstable and collapsed upon standing at room temperature for an hour, **P**= precipitate). Ag:L represent the metal to ligand molar ratio (**Ag**= silver, **L**= ligand).

DMSO :H_2O	**L**	**Ag:L**	NO_3^-	ClO_4^-	OTf^-	PF_6^-	BF_4^-	OAc^-
3:7	**1**	1:2	G	G*	G*	G	G	G
3:7	**2**	1:2	P	P	G	G	P	G
7:3	**3**	1:1	G	G	G	G	G	G
7:3	**4**	1:1	G*	G*	G*	G	G*	G

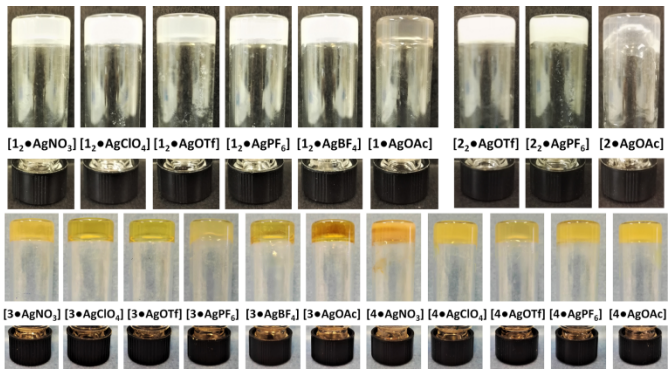

Figure 3. Photographs of gels prepared from ligands **1**-**4** with various silver salts in aqueous DMSO.

The above study revealed that all the compositions resulted in gels. However, at L:M ratio of 4:1 a weak gel was formed, gels obtained from 1:1 of ligand to silver were found to be unstable and collapsed at room temperature within *ca.* 10 minutes. However, stable gels were obtained when L:M ratio was maintained at 2:1 indicating possible tetracoordination of silver ions. Similar observation were made for ligand **2**, therefore further studies performed are using 2:1 (ligand:metal) ratio and in 3:7 DMSO:H_2O for ligands **1** and **2** (Fig. 3). The minimum gelation concentration (mgc) was found to be 0.8 wt% for both the tested ligands in 3:7 DMSO:H_2O. The gelation experiments of **1** with all the tested silver salts resulted in metallogels. Gels obtained from **1** with ClO_4^-, OTf^- counter anions were found to be unstable and collapsed to precipitate. Interestingly, ligand **2** gave metallogels only with the larger counter anions (OTf^-, PF_6^- and OAc^-) and resulted in precipitates with other silver salts (Fig. 3). The metallogelation of **1** and **2** was also observed in a mixture of DMF:H_2O (Fig. S1). However, during gelation experiment, the addition of metal salts results in precipitate and to obtain stable gels, the precipiate is redissolved by heating. The heating resulted in an immediate dark brown coloured gel that are unstable. The color change is attributed to the rapid reduction of silver ions by DMF, which is well documented in the literature.

Similarly the metallogelation of tetradentate ligands **3** and **4** were studied in varying ratio of DMSO:H_2O. Due to the solubility issues, more DMSO or DMF was needed than water. Accordingly,gelation was observed at different ratios of DMSO:H_2O as 8:2, 7:3 (Fig. 3) and 6:4 withgelation concetration is 0.4 wt% for ligands **3** and **4**. However, stable gels were obtained when 7:3 DMSO:H_2O was used. The study the effect of ligand to metal raito experiments using molar ratio of 2:1, 1:1, 1:2, 1:3 and 1:4 were studied using $AgNO_3$. When ligand to metal ratio 2:1 was used no gelation was observed (Fig. S1). However, addition of excess of $AgNO_3$, resulted in gels but unstable in nature. The optimum ligand to metal ratio to obtain stable gel was found to be 1:1. This suggests that silver (I) ions are tetracoordinated. Therefore, all the further studies were carried out in 7:3 DMSO:H_2O and 1:1 ligand to metal ratio for **3** and **4**. Ligand **3** fomed metallogels in all the tested silver salts (Table 1). Similar studies using ligand **4** revealed the metallogelation for all the tested salts, however, most of them are unstable except with PF_6^- and OAc^- anions. The above gelation studies thus indicate that ligands **1** and **3**

display similar behaviour, whereas ligands **2** and **4** show similar metallogelation abilities. Our results are in good agreement with the literature, where the effect of counteranion in metallogels have been well documented.[3a] The metallogels were found gradually loose water and undergo precipitation upon heating. Similar observation has been reported for other coodination polymer metallogels in the literature.[16b] The effect of temperature on gels can also be monitored using variable temperature (VT) NMR spectroscopy.[36] Under VT ^{1}H NMR experiments, the broad signals in the gel state turn sharper upon gel melting for thermoreversible gels. On the other hand, the lack of gel-sol transition will show no significant change upon heating close to the boiling point of the solvent.

Effect of temperature on **[1_2.AgNO$_3$]** gel (DMSO-d_6:D_2O) was studied by performing VT ^{1}H NMR experiments from 30 °C–80 °C (Fig. S12) with 10 °C increment step. Ligand **1** alone in DMSO-d*6* displayed characteristic sharp peaks. However, when ligand **1** alone was measured in 3:7 DMSO:H_2O all the signals showed upfield (shielded) shift with slight broadening. Addition of Ag(I) in the form of $AgPF_6$ resulted in gelation and signal broadening was evident (Fig. S12). Moreover, all the signals arising from ligands showed downfield (deshielded) shift upon adding silver salt. Increasing the temperature showed increasingly sharp peaks with clear splitting of all the resonance signals at 80 °C. The NMR tube showed a brownish coloured solution with precipitate at the bottom of the tube (Fig. S12). This suggests that the gel undergoes partial melting. Further, above 60 °C, there was a slight upfield shift of the signals and the position of resonance signals are close to that of the gel at room temperature suggesting that the signals observed in the gel state might be from free or mobile components. For ligand **3**, upfield shift was observed when 7:3 DMSO-d_6-D_2O was used compared to that of DMSO-d_6 alone. Addition of silver salt no prominent signals were observed. Upon heating above 50 °C signals were visible and even at 90 °C they remained broad (Figs. S13, S14). The sample did not show any melting at 90 °C. This suggests that the gel is not undergoing gel-sol transition under the experimental conditions.

To gain further insights, 1D (^{1}H and ^{13}C) and 2D (^{1}H-^{1}H correlation NMR spectroscopy (COSY), ^{1}H-^{13}C heteronuclear multiple bond correlation (HMBC) and ^{1}H-^{15}N COSY NMR spectroscopic measurements were performed for ligands **1–4** and their Ag-complexes in solution. Upon metal complexation, a significant change in the chemical shifts for the protons was observed (see ESI for ^{1}H NMR spectral comparison). To probe the effect of metal coordination, 2D ^{1}H-^{15}N correlation spectroscopy for free ligands and their Ag-complexes were performed in DMSO-d_6.[30] Fig. 4a shows ^{1}H-^{15}N 2D-COSY of the free ligand **1** and fig. 4b of its 2:1 metal complex **[1_2●AgNO$_3$]**. ^{1}H-^{15}N 2D COSY spectrum of ligands and its Ag-complexes were measured to know metal coordination. Upon complexation, an obvious change in the chemical shift values of nitrogen atoms was observed. The nitrogen atoms (N1 and N3) of ligand **1** showed an upfield shift of 6.84 and 10.62 ppm respectively, which is a clear indication of the coordination of both the nitrogen atoms from the ligand. The NMR spectroscopic results and optimum ligand to metal ration needed for stable metallogels suggests possible tetracoordination of Ag(I) ions. This observation is further supported by single crystal X-ray structures of **1_2.AgX** showing infinite coordination polymerization directed by tetracoordinated Ag(I) ions. The 2D ^{1}H-^{15}N correlation spectra of ligand **3** and its complex **[3●AgNO$_3$]** (Fig. S7) was measured at 70 °C due to its solubility issue.

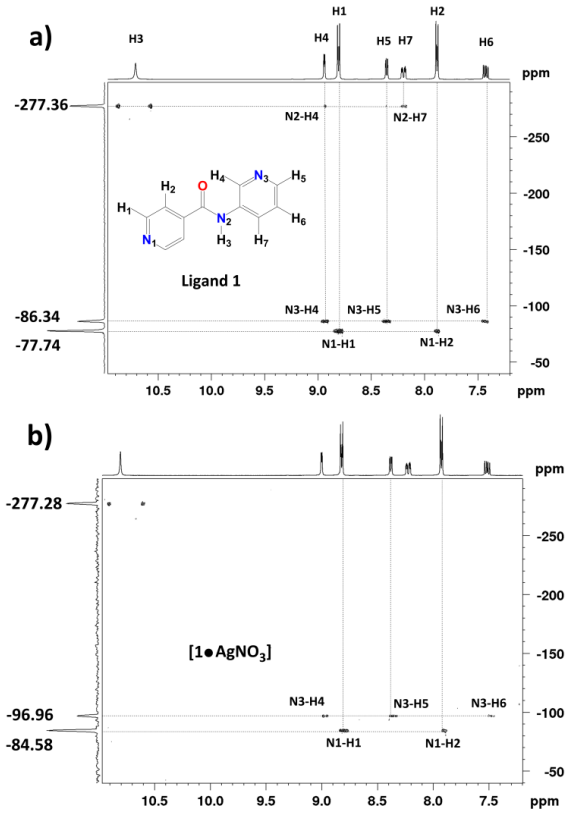

Figure 4. ^{1}H-^{15}N 2D correlated spectrum of ligand **1** and **[1_2●AgNO$_3$]** in DMSO-d_6 at 30 °C.

Even at this high temperature, a significant upfield shift from the nitrogen atoms of bipyridine (N1) and pyridine (N3) moieties was observed and the shift is 4.35 and 4.57 ppm respectively.

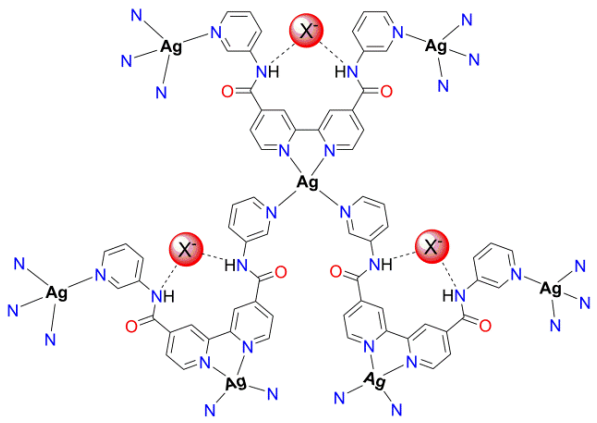

Figure 5. The proposed structure of the coordination polymer **[3●AgX]$_n$** (X= NO_3^-, ClO_4^-, OTf^-, PF_6^- and BF_4^-) in a solution and gel.

The position of the counter anion in Ag-complex was predicted based on ^{1}H NMR spectral results. The NH signals of **1** (Fig. S1) and **3** (Fig. S4) showed a downfield shift of 0.07 and 0.04 ppm respectively, in their Ag-complexes. This suggests that the presence of intermolecular H-bonding between the hydrogen atoms from amide group and counter anions, which can be seen in the solid-state structure of silver CPs with the ligand **1**. Based on the molar ratio of bipyridine ligands (**3** or **4**) to **AgX** (1:1) and the NMR spectral analysis, the complex was assigned as CP where the silver cation is tetrahedrally coordinated by one chelating bipyridine unit and two bridging pyridine rings from adjacent ligands (Fig. 5 and S13).

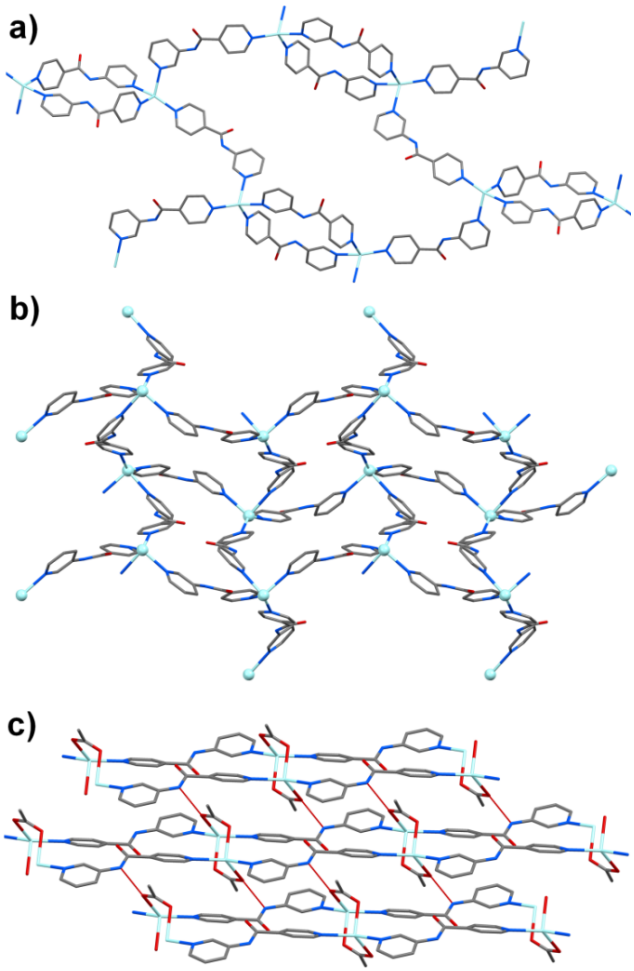

Figure 6. Crystal packing of 2D-CPs of **[1_2●AgClO$_4$] (a)**, **[1_2●AgOTf] (b)** and 1D-CP of **[1●AgOAc] (c)**. Hydrogen atoms and counter anions (ClO_4^- and $CF_3SO_3^-$) are omitted for clarity.

In order to understand detailed packing and interactions involved in coordination polymerization, we investigated the X-ray crystal structure of CPs. The crystallization of **1** with silver(I) in 7:3 or 8:2 (v/v) of DMSO:H_2O water (i.e. non-gelling conditions) leads to the formation of single crystals or precipitate. The reaction of **1** with AgX (X= ClO_4^-, OTf^- and PF_6^-) at 2:1 molar amounts gave two-dimensional coordination polymers (2D-CPs) where the silver was tetra coordinated by four individual ligand molecules.[35] The **[1_2●AgClO$_4$]** (Fig. 6a)**, [1_2●AgOTf]** (Fig. 6b)**,** and **[1_2●AgPF$_6$]**[37] (Fig. S17) were crystallized in monoclinic space group $P2_1/n$. These 2D layers interact further with each other through counter anions *via* classical N–H···O and several weak C=C–H_{Py}···O, and C=C–H_{Py}···F hydrogen bonds (Table S3) to immobilize the solvent molecules. One-dimensional ladder type coordination polymer was obtained from the reaction of **1** with AgOAc. The **[1_2●AgOAc]** (Fig. 6c) was crystallized in triclinic space group $P\bar{1}$. Similarly, each silver atom is tetra coordinated by two ligand molecules and two bridging acetate molecules to form infinite ladder type architecture. These ladders are further self-assembled to generate 2D layered structure *via* N–H···O hydrogen bonding involving amide N and acetate O atoms of the adjacent chains (N···O= 2.760(2) Å). The packing patterns in the single crystals and gel phase may be different as the gelation conditions are different from that of crystallization. In order to test this hypothesis, the powder X-ray diffraction (PXRD) was carried out for the xerogel derived from **[1_2●AgClO$_4$]**. The comparision of the PXRD pattens of the xerogel with the simulated XRD patterns of the single crystal of **[1_2●AgClO$_4$]** revelaed similar diffraction patterns (Fig. S21). This suggests that in the gel state ther exists similar packing arrangment for metal complexes.

Morphology and in-situ nanoparticle formation

The morphological features of gels were investigated using electron microscopy for all the 24 metallogels studied in this work. The transmission electron microscopy (TEM) suggested that the metallogels derived from **[1_2●AgX] and [2_2●AgX]** forms either film-like or rod-like networks depending on the counter anions (Fig. 7). Whereas, the metallogels derived from **[3●AgX]** and **[4●AgX]** showed highly entangled fibrillar networks except with $AgBF_4$. The most interesting finding from this work is the *in-situ* formation of ultrasmall nanoparticles (d <3 nm). Figure 7 shows representative TEM micrographs from **[1_2●AgX]** and **[3●AgX]** with various silver salts. While most of the gels showed the formation of fibers with uniformly distributed ultrasmall silver nanoparticles (d <3nm), the perchlorate and acetate furnished film-like structures with uniformly distributed nanoparticles. Larger particles (5-20 nm) was also observed in the case **[1_2●AgOAc]** gels. Whereas, the gels derived from **[3●AgX]** and **[4●AgX]** (see ESI) showed both ultrasmall and larger (5-20 nm) nanoparticles. This is also evident from the surface plasmon resonance (SPR) spectra of the gels (Fig. S21). As in the case of gels derived from **[1_2●AgX]** and **[2_2●AgX],** they show the formation of ultrasmall AgNPs uniformly distributed along the fibers and film-like materials. However, in addition to ultrasmall nanoparticles, the gels derived from **[3●AgPF$_6$]**, **[3●AgClO$_4$]** and **[3●AgBF$_4$]** also showed the formation of larger polydispersed nanoparticles. It should be noted that the pyridine, bipyridine and 1,10-phenanthroline based ligands have been explored previously for the synthesis of AgNPs using additional reducing agents with a considerable degree of uncontrolled aggregation of as formed nanoparticles.

Journal Name

ARTICLE

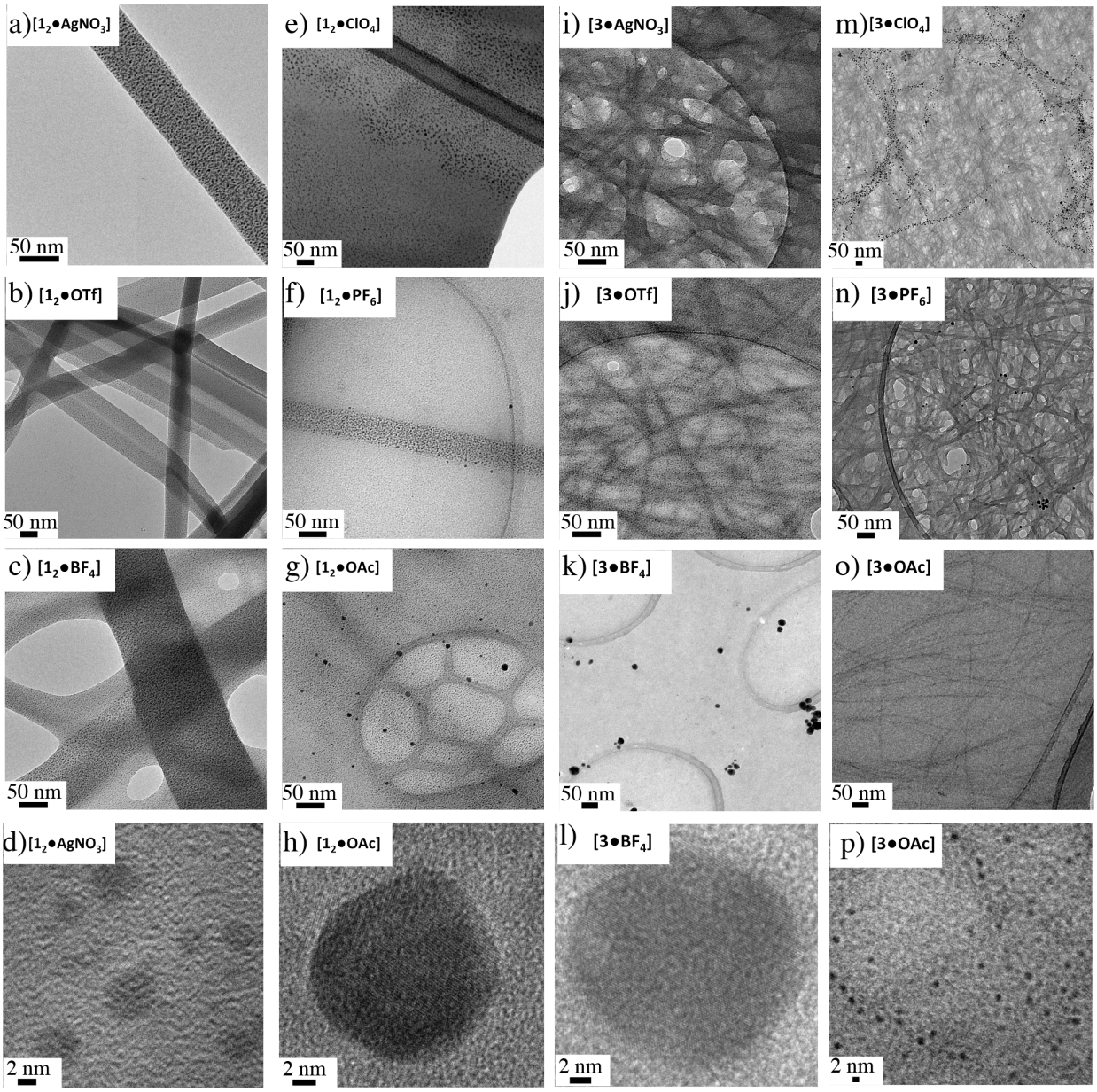

Figure 7. TEM micrographs of metallogels. Representative TEM micrographs of metallogels derived from six different salts with ligand **1** and ligand **3**, showing the gel fibers and films with *in-situ* ultrasmall nanoparticle formation. HR-TEM of individual nanoparticles shows the lattice fringes in larger nanoparticles (**h** and **l**).

Further, a vast majority of the previous report represent larger nanoparticles with d> 5 nm. Remarkably, the present work shows the formation of ultrasmall silver nanoparticles, that are well dispersed within the gel matrix and fibers. HR-TEM of small nanoparticles (Fig. 7d, p) revealed the lack of lattice fringes. This behaviour is well documented in the literature for nanoparticles having a size below 2 nm due to the non FCC packing of atoms.[38] Further, ultrasmall nanoclusters are also electron beam sensitive. However, for

larger nanoparticles, HR-TEM displayed lattice fringes (Fig.7h, I) that are typical for plasmonic silver nanoparticles.

Rheology of metallogels

The mechanical properties of metallogels are affected by ligand chemical structures, metal ions as well as the counter anions. TEM imaging suggests that the morphological features and nanoparticle formation, as well as their arrangement within the gel matrix depends on the ligand as well as the counter anions (Fig. 7). In order to gain insights on the mechanical properties of the gels, rheological measurements of the metallogels that are stabilized for 12 hours after the preparation was performed using plate and plate geometry. Accordingly, the following gels (0.8 wt%) were used for rheological measurements in duplicates, [1_2●AgX], [1_2●BF_4], [1_2●AgOAc], [1_2●PF_6], [2_2●.OTf], [3.OTf], [3.NO_3], [3.ClO_4], [3.PF_6], [3.AgOAc], [3.BF_4] and [4.AgOAc]. All other gels were unstable under the experimental conditions or upon transferring the gels for the rheological measurements. The stability of the gels was monitored using time sweep experiments, performed within the viscoelastic regime (0.1% strain) with 6.29 rad s^{-1} under the controlled temperature from 30 min to 2 h. Time sweep experiments are useful to determine the sol-gel transition by monitoring the elastic (*G`*) and loss modulus (*G``*). However, in our experiments, the pre-stabilized gels were used. For all the gels *G´* was found to be an order of magnitude higher than *G"* indicating the viscoelastic nature of the materials and the gels remained stable under the experimental conditions (Fig. 8). Similarly, the frequency sweep experiments showed that *G`* of the gels is higher than *G``*, confirming that the materials under study are viscoelastic in nature. For a given ligand the strength of the gels depends strongly on the counter anion. For metallogels derived from ligand 1, [1_2●AgX] the elastic modulus G´ was found to follow the order BF_4>PF_6>NO_3>OAc with values of 69, 60, 49 and 11 Pa, respectively (see Supporting Information, Fig. S18). Further, for a given silver salt the gel strength strongly depends on the ligand chemical structure. When AgOAc was used as silver salt the metallogels derived from ligand **4** was found to be strongest and those with ligand **1** was found to be relatively weak. The *G´* values of 406, 43 and 11 Pa, for [4●AgOAc], [3●AgOAc]and [1_2●AgOAc], respectively (see Supporting Information, Fig. S18).

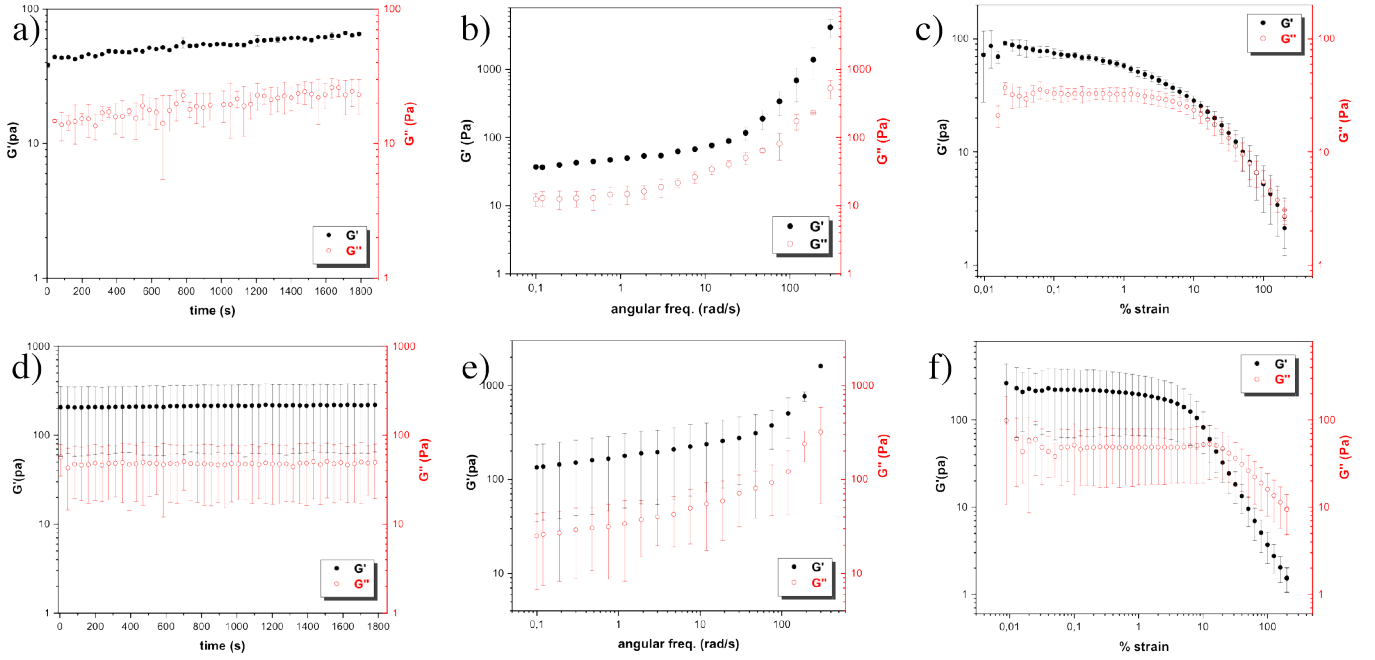

Figure 8. Selected rheological properties of metallogels. **a-c**) time sweep, frequency sweep and strain sweep experiments of **[1_2●$AgNO_3$]**. **d-f**) time sweep, frequency sweep and strain sweep experiments of **[3●$AgNO_3$]**. Filled black circles represent the storage modulus (*G´*) and empty red circles represent the loss modulus (*G´´*).

Photoluminescence

Another interesting finding in our study is the self-assembly induced photoluminescence displayed by all the metallogels studied in this work. Accordingly, the photoluminescence properties of metallogels prepared from ligands **1–4** with **AgX** in a mixture of DMSO and water were investigated. We used the $AgPF_6$ since it resulted in stable gels upon complexation with all the ligands (Table 1). All the gels displayed emission in the visible range upon photoexcitation at 300 nm (see Fig. S19a).‡ Emission measurements at different temperatures revealed that the luminescence intensity decreases upon heating of the gels (Fig. 9, Fig. S19b,c), indicating a key role of gelation in their luminescent properties.

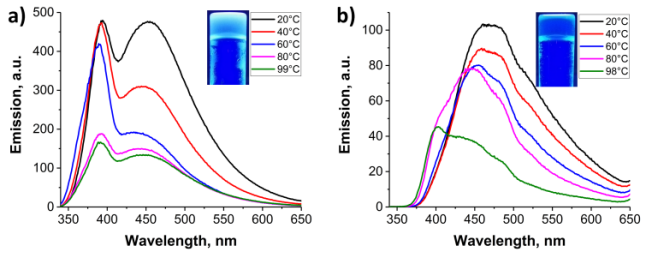

Figure 9. Variable temperature emission spectra of the coordination polymers **[1₂●AgPF₆]** (a) and **[3●AgPF₆]** (b) under excitation at 300 nm

No significant influence of the anion on luminescence was observed within PF_6 and NO_3 series (Fig. S19e,f). Comparison of the emission spectra of the gel prepared from ligand **2** alone and metallogel **[2₂●AgPF₆]** (Fig. S19d) reveals essentially the same emission wavelength, even though the emission intensity of the metallogel is several orders of magnitude lower, probably facilitated by silver(I) singlet-triplet transitions.[39] This allows for the preliminary assignment of luminescence of the metallogels understudy to intraligand π*-π or π*-n transitions.

This suggestion is also supported by a similarity between emission spectra of solid **1** and **2** (Fig. S20) and their silver metallogels, which has also been observed for other **1**-based coordination polymers.[39] At the same time, **3** and **4** based metallogels display red-shifted emission compared to pure solid ligands. This observation can be attributed to chelation of silver atoms by bipyridyl moieties, resulting in the shift of luminescence emission.

Conclusions

Metallogels are the continuously evolving area in metallosupramolecular chemistry. Silver(I) coordinated metallogels offers many additional properties such as spontaneous *in-situ* silver nanoparticle formation, optical and mechanical properties. They are also model systems to understand the structural details, interactions involved in the self-assembly as well as gelation. This work demonstrates that structurally simple pyridyl and bipyridyl amides lead to an unprecedented self-assembly induced gelation, photoluminescence as well as rapid access to ultrasmall nanoparticles. The noble metal ultrasmall nanoparticles are gaining considerable attention in recent years because of their unique size and shape dependent optical properties and possibilities to construct hierarchical colloidal superstructures. The structural details obtained by X-ray crystallography studies are useful towards the rational design of new gelators with novel functionalities.

Experimental Section

Metal Complexes

[1₂●AgNO₃]: ^{1}H NMR (300 MHz, DMSO-d_6) δ 10.78 (s, 1H), 8.99 (d, 1H), 8.82 (dd, 2H), 8.37 (dd, 1H), 8.22 (dq, 1H), 7.92 (dd, 2H), 7.50 (q, 1H). ^{13}C NMR (75 MHz, DMSO-d_6) δ 164.32, 150.70, 145.61, 14.42, 141.64, 135.65, 128.41, 124.17, 121.88. ^{1}H-^{15}N COSY NMR (DMSO-d_6 at 30 °C) δ -84.58 (Carbonyl pyridine N^C), -96.96 (amino pyridine N^N) and -277.29 (amide nitrogen N^A).

[2₂●AgNO₃]: ^{1}H NMR (300 MHz, DMSO-d_6) δ 10.95 (s, 1H), 8.83 (dd, 2H), 8.54 (dd, 2H), 7.89 (dd, 2H), 7.86 (dd, 2H).

[3●AgNO₃]: ^{1}H NMR (300 MHz, DMSO-d_6) δ 10.94 (s, 1H), 9.00 (d, 2H), 8.96 (d, 1H), 8.39 (dd, 1H), 8.24 (dq, 1H), 8.05 (dd, 1H), 7.48 (q, 1H). ^{13}C NMR (75 MHz, DMSO-d_6 at 80 °C) δ 163.94, 154.95, 149.89, 144.92, 142.79, 142.21, 134.94, 127.62, 123.12, 121.95, 118.56.

^{1}H NMR (500 MHz, DMSO-d_6 at 70 °C) δ 10.80 (s, 1H), 8.99 (d, 2H), 8.95 (d, 1H), 8.38 (dd, 1H), 8.22 (dq, 1H), 8.03 (dd, 1H), 7.46 (q, 1H). ^{1}H-^{15}N COSY NMR (DMSO-d_6 at 70 °C) δ -64.35 (Bipy N^B), -67.23 (Py N^P) and -253.16 (Amide N^A).

[4●AgNO₃]: No solubility was found.

Gelation procedure

In a typical gelation experiment, an appropriate amount of solid ligand (**1**–**4**) was placed in a test tube (*l*=45 mm, *d*=15 mm) and dissolved in DMSO upon heating, whereupon an aqueous solution of the corresponding silver salt (AgX) was added to reach a final volume of 1.0 mL. The mixture was then cooled down to room temperature, which furnished a translucent/transparent gel or precipitate depending on the ligand and silver salt.

X-ray crystallography

The single crystals of **4** and silver CPs from **1** were immersed in cryo-oil, mounted in a MiTeGen loop and measured at 120°C. The X-ray diffraction data were collected on an Agilent Technologies Supernova diffractometer using Mo Kα radiation. The *CrysAlisPro*[40] program packages were used for cell refinements and data reductions. Structures were solved by intrinsic phasing *SHELXT*[41] program. Analytical or multi-scan absorption correction was applied to all data and structural refinements were carried out using *SHELXL*[41] and Olex2 graphical user interface[42] software. The crystallographic details are given in the supplementary material.

Transmission electron microscopy (TEM)

The transmission electron microscopy (TEM) images were collected using FEI Tecnai G2 operated at 120 kV and JEM 3200FSC field emission microscope (JEOL) operated at 300 kV in bright field mode with Omega-type Zero-loss energy filter. The images were acquired with GATAN DIGITAL MICROGRAPH software. The TEM samples were prepared by placing 3.0 µL of the gel on to a 300 mesh copper grid with holey carbon support film. The TEM grids were plasma cleaned prior to use. The samples were dried under ambient condition prior to imaging.

Rheological Measurements

TA AR2000 stress-controlled rheometer equipped with 20 mm steel plate and a Peltier heated plate was used for rheological characterization. The gels prepared in 8 mL vials with screw cap were stabilized for 12 h and transferred to the rheometer by scooping. The measuring setup was covered with a sealing lid in order to prevent evaporation during the measurements. Measurements were performed using 0.1% strain and the oscillation frequency of 6.289 rad/s^{-1} (1 Hz) at 20 °C unless otherwise noted. All the measurements were carried out in duplicate and

the rheological data were analyzed using the TA Universal Analysis software.

Photoluminescence measurements

Uvasol grade DMSO (Merck) was used for all optical measurements. Photoluminescence spectra were measured using Varian Cary Eclipse Fluorescence Spectrophotometer. Gel samples were prepared directly in 1 cm quartz cuvettes with care to produce as transparent gels as possible. Samples of the solid ligands were measured as thin layers of grinded powder pressed between quartz plates

Conflicts of interest

"There are no conflicts to declare".

Acknowledgements

TR and MH kindly acknowledge the financial support from the Academy of Finland (M.H. Proj. no. 295581). Academy of Finland, Centre of Excellence in Molecular Engineering of Biosynthetic Hybrid Materials (HYBER, 2014–2019) and the Aalto University Nanomicroscopy Center (Aalto-NMC) is kindly acknowledged for the use of its facilities. COST Action 1302 "Smart Inorganic Polymers" is also acknowledged as a valuable source of inspiration.

Notes and references

ǂ Low emission intensity and slight dependence of emission on orientation of the gel sample were observed due to low transparency of the gels. All emission spectra of the gels displayed emission band with maxima at 362 and 393 nm, which is attributed to solvent admixture and its intensity depends on the sample transparency.

1 S. Leininger, B. Olenyuk, and P. J. Stang, *Chem. Rev*. **2000**, *100*, 853-908.
2 S. Kitagawa, R. Kitaura, and S. Noro, *Angew. Chem. Int*. Ed. **2004**, *43*, 2334-2375.
3 a) M.-O. M. Piepenbrock, G. O. Lloyd, N. Clarke, and J. W. Steed. *Chem. Rev*, **2010**, *110*, 1960-2004; b) Y. He, Z. Bian, C. Kang, and L. Gao, *Chem. Commun*. **2010**, *46*, 5695-5697; *Chem. Commun*. **2011**, *47*, 1589-1591; c) L.-J. Chen, Y.-Y. Ren, N.-W. Wu, B. Sun, J.-Q. Ma, L. Zhang, H. Tan, M. Liu, X. Li, H.-B. Yang, *J. Am. Chem. Soc*. **2015**, *137*, 11725-11735.
4 S. Bhowmik, B. N. Ghosh, and K. Rissanen, *Org. Biomol. Chem*. **2014**, *12*, 8836-8839.
5 a) K. Chen, L. Tang, Y. Xia, and Y. Wang, *Langmuir*. **2008**, *24*, 13838-13841; b) P. Sutar, and T. K. Maji, *Chem. Commun*. **2016**, *52*, 8055-8074.
6 a) J. B. Beck and S. J. Rowan, *J. Am. Chem. Soc*. **2003**, *125*, 13922-13923; b) X. Yan, D. Xu, X. Chi, J. Chen, S. Dong, X. Ding, Y. Yu, and F. Huang, *Adv. Mater*. **2012**, *24*, 362-369.
7 J. Zhang, C.-Y. Su, *Coord. Chem. Rev*. **2013**, 257, 1373-1408.
8 A. Y. -Y. Tam, K. M.-C. Wong, and V. W.-W. Yam, *J. Am. Chem. Soc*. **2009**, *131*, 6253-6260.
9 a) X. Yu, L. Chen, M. Zhang, and T. Yi, *Chem. Soc. Rev*. **2014**, *43*, 5346-5371; b) A. V. Zhukhovitskiy, M. Zhong, E. G. Keeler, V. K. Michaelis, J. E. P. Sun, M. J. A. Hore, D. J. Pochan, R. G. Griffin, A. P. Willard, J. A. Johnson, *Nat. Chem*. **2016**, *8*, 33-41.
10 a) M. Burnworth, L. Tang, J. R. Kumpfer, A. J. Duncan, F. L. Beyer, G. L. Fiore, S. J. Rowan, and C. Weder, *Nature*. **2011**, *472*, 334-337; b) G. E. Giammanco, C. T. Sosnofsky, and A. D. Ostrowski, *ACS Appl. Mater. Interfaces*. **2015**, *7*, 3068-3076; c) M. Mauro, S. Bellemin-Laponnaz, and C. Cebrian, *Chem. Eur. J*. **2017**, ***23***, 17626-17636.
11 a) S.-I. Kawano, N. Fujita, and S. Shinkai, *J. Am. Chem. Soc*. **2004**, *126*, 8592-8593; b) S. Sarkar, S. Dutta, S. Chakrabarti, P. Bairi, and T. Pal, *ACS Appl. Mater. Interfaces*. **2014**, *6*, 6308-6316; c) Y. Zhang, B. Zhang, Y. Kuang, Y. Gao, J. Shi, X. X. Zhang, and B. Xu, *J. Am. Chem. Soc*. **2013**, *135*, 5008-5011; d) K.Mitsumoto, J. M. Cameron, R. -J. Wei, H. Nishikawa, T. Shiga, M. Nihei, G. N. Newton, H. Oshio, *Chem. Eur. J*. **2017**, *23*,1502-1506.
12 C. Wang, D. Zhang, and D. Zhu *J. Am. Chem. Soc*. **2005**, *127*, 16372-16373.
13 T. Kishida, N. Fujita, K. Sada, and S. Shinkai, *Langmuir*. **2005**, *21*, 9432-9439.
14 Y. Cho, J. H. Lee, J. Jaworski, S. Park, S. S. Lee and J. H. Jung, *New. J. Chem*. **2012**, *36*, 32-35.
15 a) J. H. Lee, S. Kang, J. Y. Lee and J. H. Jung, *Soft Matter*. **2012**, ***8***, 6557-6563; b) L. Yan, L. Shen, M. Lv, W. Yu, J. Chen, S. Wang, X. Fu and Z. Ye, *Chem. Commun*. **2015**, ***51***, 17627-17629; c) S. Ganta and D. K. Chand, *Dalton Trans*. **2015**, *44*, 15181-15188; d) S.-L. Yim, H.-F. Chow, M.-C. Chan, C.-M. Che, K.-H. Low, *Chem. Eur. J*. **2013**, *19*, 2478-2486
16 P. Casuso, P. Carrasco, I. Loinaz, G. Cabanero, H. J. Grande and I. Odriozola, *Soft Matter*. **2011**, *7*, 3627-3633.
17 a) J. J. Marrero-Tellado and D. D. Díaz, *CrystEngComm*. **2015**, *17*, 7978-7985; b) A. Husain, R. Parveen, and P. Dastidar, *Cryst. Growth Des*. **2015**, *15*, 5075-5085.
18 a) K. K. Kartha, V. K. Praveen, S. S. Babu, S. Cherumukkil, and A. Ajayaghosh, *Chem. Asian. J*. **2015**, *10*, 2250-2256; b) R. Tatikonda, S. Bhowmik, K. Rissanen, M. Haukka, and M. Cametti, *Dalton Trans*. **2016**, *45*, 12756-12762.
19 a) N. N. Adarsh, P. Sahoo, and P. Dastidar, *Cryst. Growth Des.* **2010**, *10*, 4976-4986; b) H. Bunzen, Nonappa, E. Kalenius, S. Hietala, and E. Kolehmainen, *Chem. Eur. J*. **2013**, *19*, 12978-12981.
20 R. G. Weiss, *J. Am. Chem. Soc*. **2014**, *136*, 7519-7530.
21 A. Y.-Y. Tam, and V. W.-W. Yam, *Chem. Soc. Rev*. **2013**, *42*, 1540-1567.
22 a) S. Bhowmik, B. N. Ghosh, V. Marjomaki, and K. Rissanen, *J. Am. Chem. Soc*. **2014**, *136*, 5543-5546. (b) Q. Lin, T.-T. Lu, X. Zhu, B. Sun, Q.-P. Yang, T.-B. Wei and Y.-M. Zhang, *Chem. Commun*. **2015**, *51*, 1635-1638.
23 a) P. Chen, Q. Li, S. Grindy, and N. Holten-Andersen, *J. Am. Chem. Soc*. **2015**, *137*, 11590-11593; b) P. Sutar, V. M. Suresh, and T. K. Maji, *Chem. Commun*. **2015**, *51*, 9876-9879; c) K. Hong, Y. K. Kwon, J. Ryu, J. Y. Lee, S. H. Kim, and K. H. Lee, *Sci. Rep*. **2016**, *6, 29805.* Doi:10.1038/srep29805; d) P. Sutar, and T: K. Maji, *Inorg. Chem*. **2017**, *56*, 9417-9425.
24 M. J. Bryant, J. M. Skelton, L. E. Hatcher, C. Stubbs, E. Madrid, A. R. Pallipurath, L. H. Thomas, C. H. Woodall, J. Christensen, S. Fuertes, T. P. Robinson, C. M. Beavers, S. J. Teat, M. R. Warren, F. Pradaux-Cassiano, A. Walsh, F. Marken, D. R. Carbery, S. C. Parker, N. B. McKeown, R. Malpass-Evans, M. Carta, and P. R. Raithby, *Nat. Commun.* **2017**, *8,* 1800. Doi:10.1038/s41467-017-01941-2.
25 L. Arnedo-Sanchez, Nonappa, S. Bhowmik, S. Hietala, R. Puttreddy, M. Lahtinen, L. DeCola, and K. Rissanen, *Dalton Trans*. **2017**, *46*, 7309-7316.
26 a) B. Xing, M.-F. Choi and B. Xu, *Chem. Eur. J*. **2002**, *8*, 5028-5032; b) Y.-R. Liu, L. He, J. Zhang, X. Wang, and C.-Y. Su, *Chem. Mater*. **2009**, *21*, 557-563.
27 L. Qin, P. Wang, Y. Guo, C. Chen, and M. Liu, *Adv. Sci*. **2015**, *2*, 1500134. DOI: 10.1002/advs.201500134.

28 a) M.-O. M. Piepenbrock, N. Clarke, and J. W. Steed, *Soft Matter*. **2011**, *7*, 2412-2418; b) H. Svobodová, Nonappa, M. Lahtinen, Z. Wimmer, and E. Kolehmainen, *Soft Matter.* **2012**, *8*, 7840-7847; c) M. Cametti and Z. Džolić, *Chem. Commun*. **2014**, *50*, 8273-8286.
29 P. Rajamalli, P. Malakar, S. Atta, and E. Prasad, *Chem. Commun*. **2014**, *50*, 11023-11025.
30 a) K. Nath, A. Husain, and P. Dastidar, *Cryst. Growth Des*. **2015**, *15*, 4635-4645; b) M. Paul, K. Sarkar and P. Dastidar, *Chem. Eur. J*. **2015**, *21*, 255-268.
31 R. Tatikonda, K. Bertula, N. Nonappa, S. Hietala, K. Rissanen, and M. Haukka, *Dalton Trans.* **2017**, *46*, 2793-2802.
32 (a) M. Oh and C. A. Mirkin, *Nature*. **2005**, *438*, 651-654; b) A. I. d'Aquino, Z. S. Kean, and C. A. Mirkin, *Chem. Mater*. **2017**, *29*, 10284-10288; c) X. Sun, S. Dong, and E. Wang, *J. Am. Chem. Soc.* **2005**, *127*, 13102-13103; *Chem. Soc. Rev*. **2009**, *38*, 1218-1227.
33 C. Zimmer, M. Hafner, M. Zender, D. Ammann, R. W. Hartmann, *Bioorganic Med. Chem. Lett*. **2011**, *21*, 186-190
34 D. K. Kumar, D. A. Jose, P. Dastidar, and A. Das, *Langmuir.* **2004**, *20*, 10413-10418.
35 CCDC 1823427–1823433 contains the supplementary crystallographic data for this paper.
36 a) Nonappa and E. Kolehmainen, *Soft Matter*. **2016**, *12*, 6015-6026; b) Nonappa, M. Lahtinen, B. Behera, E. Kolehmainen, and U. Maitra, *Soft Matter*. **2010**, *6*, 1748-1757; c) V. Noponen, Nonappa, M. Lahtinen, A. Valkonen, H. Salo, E. Kolehmainen, and E. Sievänen, *Soft Matter*. **2010**, *6*, 3789-3796; d) Nonappa and E. Kolehmainen, *Gels*. **2016**, *2*, 9; e) Nonappa, D. Saman, and E. Kolehmainen, *Magn. Reson. Chem*. **2015**, *53*, 256-260.
37 K. Uemura, *Inorg. Chem. Commun*. **2008**, *11*, 741-744.
38 R. Jin, C. Zeng, M. Zhou, and Y. Chen. *Chem. Rev*., **2016**, *116*, 10346–10413.
38 R. Tatikonda, E. Bulatov, E. Kalenius, and M. Haukka, *Cryst. Growth Des.* **2017**, *17*, 5918-5926.
39 a) J. A. Wilson, R. L. LaDuca, *Inorg. Chem. Acta*. **2013**, *403*, 136-141; b) T. A. Beard, J. A. Wilson, R. L. LaDuca, *Inorg. Chem. Acta*. **2017**, *466*, 30-38.
40 Rigaku Oxford Diffraction, CrysAlisPro. **2013**, Yarnton, Oxfordshire, England.
41 G. M. Sheldrick, *Acta Cryst*. **2015**, *C71*, 3-8; *Acta Cryst*. **2015**, *A71*, 3-8.
42 O. V. Dolomanov, L. J. Bourhis, R. J. Gildea, A. J. K. Howard, and H. Puschmann, *J. Appl. Cryst*. **2009**, *42*, 339-341.